Dalton Transactions

Accepted Manuscript

ROYAL SOCIETY OF CHEMISTRY

www.rsc.org/dalton

Copper-Incorporated Mono- and Di-$TeRu_5$ Metal Carbonyl Complexes: Syntheses, Structures, and an Unusual Skeletal Arrangement

Minghuey Shieh,* Chia-Yeh Miu, Kai-Jieah Hsing, Li-Fing Jang, and Chien-Nan Lin

Department of Chemistry, National Taiwan Normal University, Taipei 11677, Taiwan, Republic of China

*To whom all correspondence should be addressed. E-mail: mshieh@ntnu.edu.tw.

Abstract

Two sandwich-type Cu_3Cl- or $Cu_2\{Te_2Ru_4(CO)_{10}\}$-bridging di-$TeRu_5$ clusters, $[\{TeRu_5(CO)_{14}\}_2Cu_3Cl]^{2-}$ (**1**) and $[\{TeRu_5(CO)_{14}\}_2Cu_2\{Te_2Ru_4(CO)_{10}\}]^{4-}$ (**2**), were obtained from the reaction of $[TeRu_5(CO)_{14}]^{2-}$ with 1 equiv of $[Cu(MeCN)_4][BF_4]$ in CH_2Cl_2 or THF at 0 ^oC, respectively, depending on the solvents. The chloride-abstracted **1** was structurally characterized to have two $TeRu_5$ cores that were linked by a Cu_3Cl moiety with two Cu─Cu bonds. If the reaction was carried out in a molar ratio of 1: 2 at 0 or 30 ^oC in CH_2Cl_2, the structural isomers $[TeRu_5(\mu\text{-}CO)_2(CO)_{12}(CuMeCN)_2]$ (**3a**) and $[TeRu_5(\mu\text{-}CO)_3(CO)_{11}Cu_2(MeCN)_2]$ (**3b**) were produced, respectively, as the major product. Cluster **3a** displayed a $TeRu_5$ core with two adjacent Ru_3 triangles each capped by a μ_3-Cu(MeCN) fragment, while **3b** contained a $TeRu_5$ core with one triangle Ru_3 plane capped by a $Cu_2(MeCN)_2$ fragment with two Cu atoms covalently bonded. Upon heating, the isomerization of **3a** into **3b** proceeded to undergo an unusual skeletal arrangement of Cu(MeCN) and migration of CO, with the $TeRu_5$ core remaining intact. Electrochemical study revealed that **3a** and **3b** each exhibited only one oxidation while cluster **1** had two consecutive oxidations, suggesting significant electronic communication between the two $TeRu_5$ metal cores in **1** via the Cu_3 moiety. This work describes the facile synthesis of a series of semiconducting Cu_x-bridging Te─Ru carbonyl clusters, in which the incorporation of the

Cu_x fragments has significantly influenced their resultant structures, rearrangements, and electronic properties, which was further elucidated by DFT calculations.

Introduction

Heteronuclear clusters containing group 8 and 11 elements have attracted much attention because of the unusual bonding properties of the bridging M_x fragments (M = Cu, Ag, Au) with certain degree of flexibility which resulted in novel bonding modes, differing structural features, and interesting skeletal isomerism.[1,2] Among these, several noted examples of metal skeletal rearrangements were reported by Salter and co-workers. For example, the Cu_2Ru_3 core in the hexanuclear clusters $[Cu_2Ru_4H_2(L)_n(CO)_{12}]$ (L = phosphine or diphosphine; n = 2 or 1) was shown to undergo restricted Berry pseudo-rotation in solutions by NMR studies.[1b] In fact, a variety of mono- or di-polyhedral ruthenium carbonyl clusters bonded with copper(I) ions have been reported,[1b,3] in which the Cu_x fragments were generally supported by ancillary ligands such as halides and phosphines. Nevertheless, these studies mainly focused on their syntheses and structural characterizations, but less emphasized on the skeletal rearrangements as well as the electrochemical and electronic properties affected by the incorporation of the Cu_x atoms.[1b,3]

Heterometallic Ru─Cu clusters are also known to act as potential catalysts with high catalytic activities.[4] Besides, the introduction of chalcogen atoms into ruthenium or copper complexes could enhance their catalytic performance and also form precursors to some useful solid-state materials and semiconductors.[5-7] However, the chemistry of Ru─Cu complexes

incorporated with chalcogens has remained obscure,[8,9] primarily because of the lack of practical synthetic methodologies. We recently reported stepwise routes to a series of CuX-incorporated $TeRu_5$-based clusters by the treatment of the octahedral complex, $[TeRu_5(CO)_{14}]^{2-}$, with appropriate amounts of CuX (X = halides).[9b] In the present study, in an attempt to minimize the halide effects and to study cooperative interaction between Ru and Cu metals, we further examined the reactivity of $[TeRu_5(CO)_{14}]^{2-}$ toward a different copper source, $[Cu(MeCN)_4][BF_4]$, which led to the formation of the Cu_3Cl-, $Cu_2\{Te_2Ru_4(CO)_{10}\}$-, di-Cu(MeCN)-, and $Cu_2(MeCN)_2$-bridging di- or mono-$TeRu_5$-based clusters **1**, **2**, and **3** (isomers **3a** and **3b**). Interestingly, these Cu_x-containing clusters exhibited interesting semiconducting behaviors with varied energy gaps. Moreover, the electronic communication between the two $TeRu_5$ cores in **1**, via the bridging Cu_3 moiety, and the isomerization of **3a** and **3b**, concerning the rearrangements of Cu(MeCN) and CO, have been demonstrated by their electrochemical properties and/or DFT calculations.

Results and discussion

Reaction of $[TeRu_5(CO)_{14}]^{2-}$ with $[Cu(MeCN)_4][BF_4]$ (designated as [Cu]) in a molar ratio of 1: 1 for different solvents

When the previously reported octahedral cluster $[TeRu_5(CO)_{14}]^{2-}$,[9b] was treated with [Cu] in a

molar ratio of 1: 1 in CH_2Cl_2 at 0 ^oC, the novel Cu_3Cl-linked di-$TeRu_5$-based cluster $[\{TeRu_5(CO)_{14}\}_2Cu_3Cl]^{2-}$ (**1**) was formed in 96% yield (Scheme 1). Cluster **1** was fully characterized by spectroscopic methods and single-crystal X-ray diffraction analysis. Cluster **1** can be viewed as having two $TeRu_5$ carbonyl clusters sandwiching a four-membered Cu_3Cl ring, in which two Cu─Cu bonds are covalently bonded (av. 2.54(8) Å) and two Cu atoms are weakly bonded (2.938(4) Å) which is further bridged by a Cl atom (Fig. 1). Some related examples of the Cl-bridging group 11-linked high-nuclearity ruthenium clusters, $[\{Ru_4H(CO)_{12}\}_2Cu_7Cl_3]^{2-}$,[3e] $[\{Ru_6H(CO)_{17}\}_2Cu_6Cl_2]^{2-}$,[3e] and $[\{Ru_5C(CO)_{14}\}_2Ag_3Cl]^{2-}$,[10] have been reported, where the bridging Cl atoms were found to stabilize the resultant clusters against fragmentations. To address the chloride source, a similar reaction was conducted with CH_2Br_2, which produced the known Cu_4Br_2-linked di-$TeRu_5$-based cluster $[\{TeRu_5(CO)_{14}\}_2Cu_4Br_2]^{2-}$[9b] (Scheme 1), as an oxidized product from the Cu_3Br-bridging analog, confirming that the halides were abstracted from CH_2X_2 (X = Cl, Br) in these reactions. A related study on halide abstraction from CH_2X_2 (X = Cl, Br) was also reported in the reaction with Cu(I) alkoxides and dppm, resulting in different structural types of Cu(I) halide complexes.[11] Contrary to CH_2X_2 (X = Cl, Br), the reaction of $[TeRu_5(CO)_{14}]^{2-}$ with [Cu] in THF (Scheme 1) afforded a highly charged $Cu_2\{Te_2Ru_4(CO)_{10}\}$-bridging di-$TeRu_5$-based cluster $[\{TeRu_5(CO)_{14}\}_2Cu_2\{Te_2Ru_4(CO)_{10}\}]^{4-}$ (**2**). Cluster **2** was shown by

X-ray analysis to consist of two $TeRu_5(CO)_{14}$ clusters linked by a di-Cu-bridging $Te_2Ru_4(CO)_{10}$ unit (Fig. 2), where the central octahedral Te_2Ru_4 moiety was considered to have resulted from the oxidation of $[TeRu_5(CO)_{14}]^{2-}$ by Cu(I) in THF.[9b] In addition, anion **2** easily decomposed in solution to form $[Te_2Ru_4(CO)_{10}Cu]^-$ (*m*/*z* calcd. 1005; found 1004.3), $[TeRu_5(CO)_{14}Cu]^-$ (*m*/*z* calcd. 1090; found 1090.4), and $[\{PPh_4\}\{TeRu_5(CO)_{14}\}]^-$ (*m*/*z* calcd. 1365; found 1365.2), as detected by ESI-MS analysis. These results suggested that CH_2X_2 (X = Cl or Br) acted as the halide source and the halides played an important role in stabilizing the Cu_3- or Cu_4-bridging di-$TeRu_5$-based clusters **1** and $[\{TeRu_5(CO)_{14}\}_2Cu_4Br_2]^{2-}$.

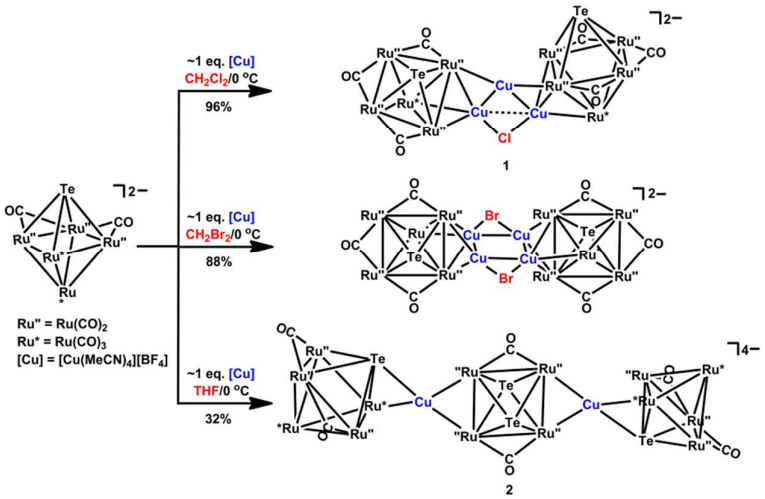

Scheme 1 Synthesis of the Cu_x-linked clusters **1** and **2**.

Reaction of $[TeRu_5(CO)_{14}]^{2-}$ with [Cu] in a molar ratio of 1: 2 at different temperatures

If $[TeRu_5(CO)_{14}]^{2-}$ was treated with [Cu] in a molar ratio of 1: 2 at 0 °C in CH_2Cl_2, the neutral Ru–Cu cluster $[TeRu_5(\mu\text{-}CO)_2(CO)_{12}(CuMeCN)_2]$ (**3a**) was produced (Scheme 2) along with a minor chloride-abstracted known complex $[\{TeRu_5(CO)_{14}\}_2Cu_4Cl_2]^{2-}$[9a] (**4**).

However, a similar reaction carried out at 30 ^{o}C formed another neutral cluster $[TeRu_5(\mu\text{-}CO)_3(CO)_{11}Cu_2(MeCN)_2]$ (**3b**) as its major product. Clusters **3a** and **3b** were structural isomers and fully characterized by spectroscopic methods and X-ray crystallographic analyses. Cluster **3a** displayed a $TeRu_5$ metal core with two μ_3-Cu(MeCN) groups each capping two neighboring triangular Ru_3 planes and two adjacent Ru─Ru bonds opposite the μ_3-Cu(MeCN) groups were each bridged by a μ-CO ligand (Fig. 3). Cluster **3b** consisted of a $TeRu_5$ core with one triangular Ru_3 plane capped by one μ_3-$Cu_2(MeCN)_2$ group, in which three Ru─Ru bonds of the Ru_4 plane were each bridged by a μ-CO ligand (Fig. 4). The existence of the two MeCN groups of **3a** and **3b** was confirmed by ^{1}H NMR experiments, revealing a singlet peak at δ2.36 and δ2.31, respectively. The values for **3a** and **3b** were close and comparable with the previously reported value for the related cluster $[Ru_6C(CO)_{16}Cu_2(MeCN)_2]$ (δ2.30).[3a]

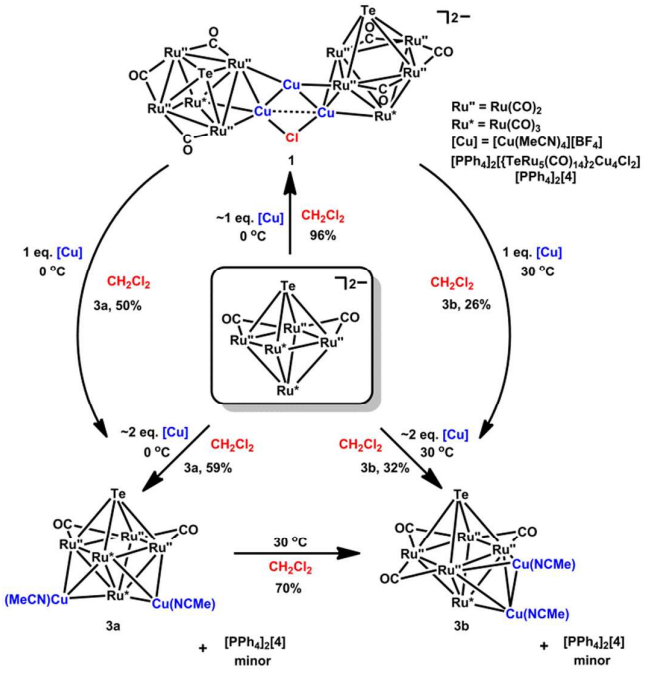

Scheme 2 Synthesis of isomers **3a** and **3b** and their transformation.

Transformations

Cu_3Cl-, di-Cu(MeCN)-, and $Cu_2(MeCN)_2$-incorporated di- or mono-$TeRu_5$-based clusters **1** and **3** (**3a**, **3b**) were systematically synthesized by fine-tuning the molar ratio of $[TeRu_5(CO)_{14}]^{2-}$ and [Cu] under different reaction conditions, and, therefore, their rational transformations were of great interest and carried out under appropriate conditions. As shown in Scheme 2, when Cu_3Cl-linking cluster **1** was treated with 1 equiv of [Cu] at 0 or 30 ^{o}C in CH_2Cl_2, the di-Cu(MeCN)- or $Cu_2(MeCN)_2$-incorporated cluster **3a** or **3b** was obtained, respectively. Cluster **3a** could further transform into its structural isomer **3b** upon heating in CH_2Cl_2, indicating cluster **3b** is a thermodynamic product. This isomerization process was recorded by variable temperature ^{1}H NMR study. When the sample of **3a** was cooled at −40

^{o}C, a sharp singlet appeared at δ2.41 which was slightly shifted to δ2.29, upon the temperature arising from ─40 to 50 ^{o}C (Fig. S1). It was noted that this skeletal rearrangement only involved the migration of the inorganic fragment Cu(MeCN), with the parent $TeRu_5$ cluster core remaining intact. Relative to ligand migrations in many other studies, such an isomerism concerning metal atom rearrangements has been rarely reported,[12] which prompted us to study the mechanism for **3a** to **3b** by DFT calculations (discussed later).

X-ray structural comparison of 1─3

According to the X-ray analysis (Fig. 1), cluster **1** displayed two $TeRu_5$-based octahedral moieties linked by a Cu_3Cl unit, in which the two $TeRu_5$ octahedra were positioned approximately in the *cis* position. In addition, the mean deviation from the least-squares plane through the four atoms, Cu_3Cl (Cu1Cu3Cu2Cl1 (67%) and Cu1Cu3aCu2Cl1 (33%)), of **1** was 0.053 or 0.097 Å, which indicated a slightly distorted Cu_3Cl tetragon. Although a similar M_3X mode was also found in $[\{Ru_5C(CO)_{14}\}_2Ag_3Cl]^{2-}$[10] and $[\{TeFe_3(CO)_9\}_2Cu_3X]^{2-}$ (X = Br, I),[13] this type of bonding in **1** was first reported in the bimetallic Ru─Cu system. On the other hand, cluster **2** was thought to have two $TeRu_5$-based octahedral clusters sandwiching a $Cu_2\{Te_2Ru_4(CO)_{10}\}$ unit via the Te─Ru edges, in which a crystallographic centre of symmetry sat at the centre of the Ru_4 plane of the central $Cu_2\{Te_2Ru_4(CO)_{10}\}$ fragment (Fig. 2). The dihedral angle between the Te1─Ru4─Cu1 and Ru6─Ru7─Cu1 planes of **2** was

68.958(4)°, where the coordination geometry around the μ_4-Cu atom of **2** was intermediate to a tetrahedral and a square-planar arrangement.

Furthermore, cluster **3a** exhibited a di-Cu(MeCN)-capping $TeRu_5$-based geometry with two neighboring triangular Ru_3 planes capped by the two Cu(MeCN) groups, while its isomer **3b** displayed a $Cu_2(MeCN)_2$-incorporated $TeRu_5$ core structure with one Ru_3 plane capped by a Cu(MeCN) group and the resultant Ru_2Cu plane further capped by another Cu(MeCN) group, where the two Cu atoms were covalently bonded (2.645(1) Å) (Fig. 3 and 4). As shown in Chart 1, these Cu_2-incorporated $TeRu_5$ octahedral clusters **3a** and **3b** could be compared to types III and IV of the related bicapped octahedral M_8 polyhedra (M = transition metals), respectively, in which they have either been theoretically predicted (types I─III) or experimentally characterized (types I─IV).[1c,14] In these studies, skeletal rearrangements between types I and II have been reported,[15] but no direct experimental or computational evidence has supported the conversion between types III and IV.[3a]

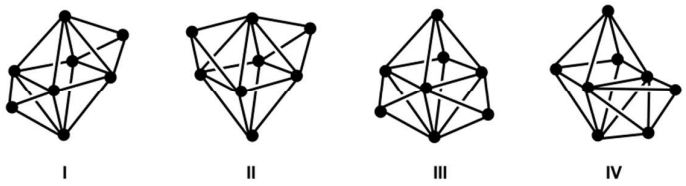

Chart 1 Bicapped octahedral polyhedra (types I─IV).

Apart from the dissimilar $TeRu_5Cu_2$ metal skeleton, the stereochemistry of the 14 CO groups in isomers **3a** and **3b** is different. Isomer **3a** contains 12 terminal COs and 2 bridging

COs, while **3b** contains 11 terminal COs and 3 bridging COs (Fig. 3 and 4). Notably, in the di-Cu(MeCN)-capping cluster **3a**, the bond distances between the Cu atom of each Cu(MeCN) fragment and the bound Ru atoms are different, with the largest difference of 0.0630(4) and 0.0310(4) Å, respectively (Table S1), implying one Cu(MeCN) fragment is more labile than the other.[12] Besides, the Cu atoms and the C atoms of the adjacent COs in **3a** were within van der Waals contacts, ranging from 2.445(3) to 3.088(3) Å, indicating weak interactions of the Cu atoms with adjacent semibridging COs and also implying the potential fluxionality of these COs. Based on these structural features, upon the heating, **3a** could easily lose one labile Cu(MeCN) moiety that then migrated to the adjacent Ru_3 plane to form **3b**, involving the Ru─Cu bond breakage and reformation, accompanied by CO migration (discussed later).

For further comparison, the average selected bond distances of **1**─**3** and related complexes are listed in Table 1.[3a,3c,9b,10,13,16,17] The Cu─Cu distances in **1** and **3b** were significantly shorter than those in the related Cu_3-[13] and Cu_2-bridging[3a,17] carbonyl clusters, respectively. Moreover, the average Ru─Ru distances of the $TeRu_5$-based clusters **1**, **3a**, and **3b** were comparatively lengthened compared with that of the parent cluster $[TeRu_5(CO)_{14}]^{2-}$,[9b,16] indicating the slightly distorted octahedral cores that could be affected by the Cu_x fragments.

Computational studies

To elucidate the unusual skeletal arrangements and electrochemical and optical properties of the Ru─Cu telluride clusters **1**, **3a**, and **3b**, DFT calculations were conducted. The computational details (See the Supplementary Information) are summarized in Tables S2-S6 as well as in Fig. 5 and Fig. S2-S4.

Skeletal arrangements

As mentioned, the cleavage and reformation of the Ru─Cu bonds and the migration of the semibridging CO were key steps in the isomerization of **3a** (with two bridging COs) to **3b** (with three bridging COs and one Cu─Cu bond), DFT calculations were employed to gain insight into the possible pathways (Fig. 5). For the initial transformation of **3a** to **I1**, the semibridging CO that had coordinated with the Ru(40) atom of **3a** was removed to bridge the adjacent Ru(42)─Ru(40) bond, resulting in the CO-migration conformation **I1**, in which two conformations, **3a** and **I1**, were found within a narrow ca. 1.4 kcal mol^{-1} energy range, suggesting a fluxional system.[18] In order to form the Cu─Cu bond, the geometry optimization was performed by the elongation of the Ru(42)─Cu(22) bond in **I1**, and was accompanied by the Cu(21)─Cu(22) bond formation (2.615 Å) to give **I2**. The resultant conformation of **I2** was thermodynamically unfavorable by 13.7 kcal mol^{-1} compared with that of **I1**. Next, **I2** was proposed in a ready state to transform into the thermodynamic product **3b** by cleavage of the Ru(43)─Cu(21) bond and a reformation of the Ru(39)─Cu(22) bond, via the transition

state, **TS**, which was only 2.4 kcal mol^{-1} higher than **I2**. The Ru─Cu bond cleavage in **I1** or **I2** was also reflected by their relatively weaker Wiberg bond indices (Table S3). This proposed mechanism was further confirmed by the potential energy surface scan calculations[19] by increasing the selected Ru(42)─Cu(22) bond of **I1** with a 0.10 Å step size to verify the **TS** linked either with the intermediates **I1** and **I2** or with product **3b**.

Electrochemical and optical properties

To explore the redox properties of **1**, **3a**, and **3b**, their electrochemical behavior was examined by cyclic voltammetry (CV) and differential pulse voltammetry (DPV). The CVs of these clusters were somewhat broad and could not be assigned unambiguously, therefore, the DPVs studies were carried out to explore the redox behavior of these clusters. Because of the one-electron oxidation at the Cu(I) center[20] (0.45 ~ 0.36 V), the irreversible desorption of Cu[21] (−0.33 ~ −0.38 V), and the interference of $[PPh_4]^+$ (−1.90 ~ −1.92 V), the DPVs profiles of **1**, **3a**, and **3b** were only discussed between 0.35 ~ −0.25 V. The electronic stoichiometry (Supplementary Information, electrochemistry details) is determined by the measurement of the peak width at half-height ($W_{1/2}$) based on the DPVs.[22] All the electrochemical data were summarized in Table 2[9b,22,23] and plotted in Fig. 6 with the details listed in the Supplementary Information, Table S7 and Fig. S5 and S6.

The DPV study showed that the di-$TeRu_5$-based cluster **1** had two one-electron

quasi-reversible oxidations, overlapped ($W_{1/2}$ = 217 mV) with the two maxima at 0.124 and 0.184 V, which contrasted with one one-electron quasi-reversible oxidation in **3** (Fig. 6 and Table 2) and other related mono-$TeRu_5$-based clusters.[9b] As revealed by DFT calculations, the HOMOs of **1**, **3a**, and **3b** had major contributions from the $TeRu_5$ cores, with some contributions from the Cu_x fragment but negligible contribution from the ancillary ligands (Cl and MeCN) (Fig. S2), suggesting that oxidation processes occurred in the $TeRu_5$ cores. According to their first oxidative potentials, the Cu_3-bridging cluster **1** was more easily oxidized than the Cu_2-incorporated isomers **3a** and **3b**, which was supported by a higher HOMO energy level (**1**, −2.22 eV; **3a**, −5.93 eV; **3b**, −5.97 eV) (Fig. S2) and by larger negative natural charges for the $TeRu_5(CO)_{14}$ core for **1** (−1.495 |e|) vs. **3a** (−1.247 |e|) and **3b** (−1.191 |e|) (Table S3). Isomer **3a** was also more easily oxidized than isomer **3b** (0.134 vs. 0.154 V), which was also supported by their HOMO energy levels and natural charges for the $TeRu_5(CO)_{14}$ core. It is interesting that when DPV data were used to calculate the comproportionation constant K_c value (log K_c = 1.0) for cluster **1**, a certain degree of electronic communication[23,24] between the two $TeRu_5$ cores via the Cu_3Cl bridge was revealed. To better understand the behavior of electronic communication, DFT calculations on the optimized geometries of the one-electron and two-electron oxidized species of **1** (**1'**, **1''**) were carried out and are summarized in Table S4. Clearly, the spin density of **1'** (S = 1/2)

was spanned over the two Ru_5 cores (0.63/0.06) and the central Cu_3 fragment (0.08), in which the small spin distribution on the Cu_3 linkage indicated the electronic coupling through the Cu_3 unit. Furthermore, the electronic structures of **1** and the parent cluster $[TeRu_5(CO)_{14}]^{2-}$ were also investigated by UV-vis spectroscopy (Fig. S7). Notably, the Cu_3-bridging cluster **1** gave two broad absorption bands, significantly red-shifted compared with those of $[TeRu_5(CO)_{14}]^{2-}$, attributable to the incorporation of the Cu_3 moiety into the $TeRu_5$ cores. Moreover, we analyzed the influence of the Cu_3 fragment in **1** by time-dependent DFT calculations (Table S5). The calculations showed that the low- and high-energy bands of cluster **1** were both due to MMCT (Ru to Cu) and "core-to-core" transitions ($\{TeRu_5(CO)_x\}$ to $\{TeRu_5(CO)_x\}$) (Fig. S3 and S4), highlighting the importance of the cooperative interaction between the Ru and Cu atoms, with little involvement of the ancillary Cl atom. As a result, the electronic delocalization of **1** via MMCT between the two $TeRu_5$ cores through the Cu_3 linkage was marked, which is consistent with our electrochemical studies.

Further, the optical properties of these ternary Te─Ru─Cu clusters in the solid state were also explored by the measurement of their solid-state diffuse reflectance spectra.[7a,7d] The reflectance spectrum each was converted to the absorption by using the Kubelka-Munk function, $F = (1-R)^2/2R$.[25,26] The band gap was determined in the F-versus-E plot, by extrapolating the linear portion of starting rising curve to zero, which provided the onset of

the absorption. As shown in Fig. S8, these binary and ternary clusters $[TeRu_5(CO)_{14}]^{2-}$, **1**, **2**, **3a**, **3b**, and **4** exhibited semiconducting behaviors with energy gaps of 1.17, 0.90, 0.91, 1.23, 1.41, and 0.93 eV, respectively, indicating that the band gaps can be moderately fine-tuned by the incorporation of copper atoms. These results suggested that our ternary Te─Ru─Cu clusters could be potentially used as solid-state precursors for useful semiconductors with varied energy gaps.[7]

Conclusion

A new family of the Cu_3Cl-, $Cu_2\{Te_2Ru_4(CO)_{10}\}$-, di-Cu(MeCN)-, and $Cu_2(MeCN)_2$-incorporated di- or mono-$TeRu_5$-based carbonyl semiconducting clusters **1**─**3** with varied energy gaps were synthesized, and their controlled transformations were achieved. Several special features are noteworthy. First, the isomerization from **3a** to **3b** involved the migration of the inorganic fragment Cu(MeCN) with Ru─Cu bond breakage and reformation, accompanied with CO migration and Cu─Cu bond formation, elucidated by DFT calculations. Second, the di-$TeRu_5$ cluster **1** possessed some degree of electronic communication, via the bridging Cu_3 linkage moiety, which was supported by DPV and UV-vis studies as well as by DFT calculations. Finally, the present work provided facile routes to Cu_x-incorporated $TeRu_5$-based ternary clusters, in which their skeletal arrangements and electronic properties

were significantly influenced by the cooperative interaction between the Ru and Cu metals.

Experimental part

Materials and methods

All reactions were performed under an atmosphere of pure nitrogen using standard Schlenk techniques.[27] Solvents were purified, dried, and distilled under nitrogen prior to use. PPh_4BF_4 (ACROS) was used as received. Complexes $[PPh_4]_2[TeRu_5(CO)_{14}]$[9b] and $[Cu(MeCN)_4][BF_4]$[28] were prepared according to the published method. The infrared spectra were recorded on a Perkin-Elmer Paragon 1000 IR spectrometer as solutions in CaF_2 cells. The attenuated total reflectance (ATR) spectra were recorded on a Perkin-Elmer Frontier FTIR Spectrometer. The NMR spectra were obtained on a Bruker AV 400 at 400.13 MHz for ^1H. The variable temperature ^1H NMR spectra were recorded on a Bruker AV 600 at 600.17 MHz for ^1H. ^1H chemical shifts are reported in parts per million and were referenced internally with respect to the solvent resonances (^1H, δ = 7.26 for $CDCl_3$-*d*). Elemental analyses of C, H, and N were performed on a Perkin-Elmer 2400 analyzer at the NSC Regional instrumental Center at National Taiwan University, Taipei, Taiwan. ESI-MS spectra were obtained on a Thermo Finnigan LCQ Advantage mass spectrometer.

Reaction of $[PPh_4]_2[TeRu_5(CO)_{14}]$ with $[Cu(MeCN)_4][BF_4]$ (1: ~ 1) at 0 ^oC in

CH_2Cl_2. CH_2Cl_2 (20 mL) was added to a mixture of $[PPh_4]_2[TeRu_5(CO)_{14}]$ (0.30 g, 0.18 mmol) and $[Cu(MeCN)_4][BF_4]$ (0.049 g, 0.16 mmol). The mixture was stirred at 0 ^oC for 1 h to give a yellowish-brown solution, which was filtered, followed by removal of the solvent under vacuum. The precipitate was washed with deionized water and MeOH several times and extracted with CH_2Cl_2, and was then recrystallized with $Et_2O/MeOH/CH_2Cl_2$ to give a yellowish-brown sample of $[PPh_4]_2[\{TeRu_5(CO)_{14}\}_2Cu_3Cl]$ ($[PPh_4]_2$[**1**]) (0.15 g, 0.051 mmol) (yield: 96% based on $[Cu(MeCN)_4][BF_4]$). IR (ν_{CO}, CH_2Cl_2): 2045 (w), 2002 (vs, br), 1814 (w), 1766 (w) cm^{-1}. Anal. Calcd for $C_{76}H_{40}ClCu_3O_{28}P_2Ru_{10}Te_2$: C, 30.89; H, 1.36. Found: C, 30.88; H, 1.39. Negative ion ESI-MS: *m*/*z* 1139.0 (calcd: 1139). Crystals of $[PPh_4]_2$[**1**] suitable for X-ray analysis were grown from hexanes/Et_2O/THF at 4 ^oC.

Reaction of $[PPh_4]_2[TeRu_5(CO)_{14}]$ with $[Cu(MeCN)_4][BF_4]$ (1: ~ 1) at 0 ^oC in CH_2Br_2. CH_2Br_2 (20 mL) was added to a mixture of $[PPh_4]_2[TeRu_5(CO)_{14}]$ (0.45 g, 0.26 mmol) and $[Cu(MeCN)_4][BF_4]$ (0.063 g, 0.20 mmol). The mixture was stirred at 0 ^oC for 1 h to give a yellowish-brown solution, which was filtered, followed by removal of the solvent under vacuum. The precipitate was washed with de-ionized water and ether several times and extracted with THF, and was then recrystallized with Et_2O/MeOH/THF to give a yellow-brown sample of $[PPh_4]_2[\{TeRu_5(CO)_{14}\}_2Cu_4Br_2]$[9b] (0.14 g, 0.044 mmol) (yield: 88% based on $[Cu(MeCN)_4][BF_4]$). IR (ν_{CO}, THF): 2046 (w), 2015 (s, sh), 1996 (vs), 1816 (w)

cm^{-1}.

Reaction of $[PPh_4]_2[TeRu_5(CO)_{14}]$ with $[Cu(MeCN)_4][BF_4]$ (1: ~ 1) at 0 ^oC in THF. THF (20 mL) was added to a mixture of $[PPh_4]_2[TeRu_5(CO)_{14}]$ (0.35 g, 0.21 mmol), $[Cu(MeCN)_4][BF_4]$ (0.053 g, 0.17 mmol), and PPh_4BF_4 (0.16 g, 0.405 mmol). The mixture was stirred at 0 ^oC for 20 min to give a yellowish-brown solution, which was filtered, followed by removal of the solvent under vacuum. The precipitate was washed with deionized water and MeOH several times and extracted with THF, and was then recrystallized with Et_2O/MeOH/THF to give a yellowish-brown sample of $[PPh_4]_4[\{TeRu_5(CO)_{14}\}_2Cu_2\{Te_2Ru_4(CO)_{10}\}]$ ($[PPh_4]_4$[**2**]) (0.078 g, 0.017 mmol) (yield: 32% based on Te). IR (ν_{CO}, ATR): 2031 (w), 1954 (vs), 1924 (vs), 1904 (vs), 1770 (m), 1586 (w) cm^{-1}. Anal. Calcd for $C_{134}H_{80}Cu_2O_{38}P_4Ru_{14}Te_4$: C, 35.97; H, 1.80. Found: C, 36.28; H, 2.06. Crystals of $[PPh_4]_4$[**2**]·3Et_2O suitable for X-ray analysis were grown from Et_2O/MeOH/THF at room temperature.

Reaction of $[PPh_4]_2[TeRu_5(CO)_{14}]$ with $[Cu(MeCN)_4][BF_4]$ (1: ~ 2) at 0 ^oC in CH_2Cl_2. CH_2Cl_2 (20 mL) was added to a mixture of $[PPh_4]_2[TeRu_5(CO)_{14}]$ (0.38 g, 0.22 mmol) and $[Cu(MeCN)_4][BF_4]$ (0.13 g, 0.41 mmol). The mixture was stirred at 0 ^oC for 2 h to give a yellowish-brown solution, which was filtered, followed by removal of the solvent under vacuum. The precipitate was washed with de-ionized water and MeOH several times

and extracted with Et_2O, and was then recrystallized with hexanes/CH_2Cl_2 to give a yellowish-brown sample of [$TeRu_5(\mu$-$CO)_2(CO)_{12}(CuMeCN)_2$] (**3a**) (0.15 g, 0.12 mmol) (yield: 59% based on [$Cu(MeCN)_4$][BF_4]). IR (ν_{CO}, CH_2Cl_2): 2050 (w), 2032 (s), 2005 (vs), 1952 (m), 1830 (w), 1809 (vw) cm^{-1}. Anal. Calcd for $C_{18}H_6Cu_2N_2O_{14}Ru_5Te$: C, 17.52; H, 0.49; N, 2.27 Found: C, 17.20; H, 0.49; N, 2.12. ^{1}H NMR (400 MHz, $CDCl_3$, 298 K, ppm): δ 2.36 (s, C*H*$_3$CN). Mp: 190 ^{o}C dec. Crystals of **3a** suitable for X-ray analysis were grown from Et_2O/CH_2Cl_2 at 4 ^{o}C. The residue was then extracted with CH_2Cl_2 to give the minor product $[PPh_4]_2$[**4**][9b] (0.052 g, 0.017 mmol). IR (ν_{CO}, CH_2Cl_2): 2050 (w), 2019 (s, sh), 2002 (vs), 1960 (m), 1825 (w) cm^{-1}.

Reaction of $[PPh_4]_2[TeRu_5(CO)_{14}]$ with $[Cu(MeCN)_4][BF_4]$ (1: ~ 2) at 30 ^{o}C in CH_2Cl_2. CH_2Cl_2 (20 mL) was added to a mixture of $[PPh_4]_2[TeRu_5(CO)_{14}]$ (0.47 g, 0.28 mmol) and $[Cu(MeCN)_4][BF_4]$ (0.16 g, 0.51 mmol). The mixture was stirred at 30 ^{o}C for 6 h to give a yellowish-brown solution, which was filtered, followed by removal of the solvent under vacuum. The precipitate was washed with de-ionized water and MeOH several times and extracted with Et_2O, and was then recrystallized with hexanes/CH_2Cl_2 to give a yellowish-brown sample of [$TeRu_5(\mu$-$CO)_3(CO)_{11}Cu_2(MeCN)_2$] (**3b**) (0.10 g, 0.081 mmol) (yield: 32% based on [$Cu(MeCN)_4$][BF_4]). IR (ν_{CO}, CH_2Cl_2): 2060 (w), 2033 (s), 2005 (vs), 1954 (m), 1831 (w), 1810 (vw) cm^{-1}. Anal. Calcd for $C_{18}H_6Cu_2N_2O_{14}Ru_5Te$: C, 17.52; H,

0.49; N, 2.27. Found: C, 17.48; H, 0.83; N, 2.31. ^{1}H NMR (400 MHz, $CDCl_3$, 298 K, ppm): δ 2.31 (s, C*H*$_3$CN). Mp: 210 ^{o}C dec. Crystals of **3b**·0.5CH_2Cl_2 suitable for X-ray analysis were grown from hexanes/Et_2O/THF at room temperature. The residue was then extracted with CH_2Cl_2 to give the minor product $[PPh_4]_2$[**4**][9b] (0.044 g, 0.014 mmol).

Conversion of $[PPh_4]_2$[1] to 3a and $[PPh_4]_2$[4]. CH_2Cl_2 (20 mL) was added to a mixture of $[PPh_4]_2$[**1**] (0.39 g, 0.13 mmol) and $[Cu(MeCN)_4][BF_4]$ (0.042 g, 0.13 mmol). The resultant solution was stirred at 0 ^{o}C for 1 h to give a yellowish-brown solution, which was filtered, followed by removal of the solvent under vacuum. The precipitate was washed with de-ionized water and MeOH several times and extracted with Et_2O, and was then recrystallized with hexanes/CH_2Cl_2 to give a yellowish-brown sample of **3a** (0.16 g, 0.13 mmol) (yield: 50% based on $[Cu(MeCN)_4][BF_4]$. The residue was then extracted with CH_2Cl_2 to give the minor product $[PPh_4]_2$[**4**][9b] (0.071 g, 0.023 mmol).

Conversion of $[PPh_4]_2$[1] to 3b and $[PPh_4]_2$[4]. CH_2Cl_2 (20 mL) was added to a mixture of $[PPh_4]_2$[**1**] (0.42 g, 0.14 mmol) and $[Cu(MeCN)_4][BF_4]$ (0.045 g, 0.14 mmol). The resultant solution was stirred at 30 ^{o}C for 1 h to give a yellowish-brown solution, which was filtered, followed by removal of the solvent under vacuum. The precipitate was washed with de-ionized water and MeOH several times and extracted with Et_2O, and was then recrystallized with hexanes/CH_2Cl_2 to give a yellowish-brown sample of **3b** (0.091 g, 0.074

mmol) (yield: 26% based on $[Cu(MeCN)_4][BF_4]$). The residue was then extracted with CH_2Cl_2 to give the minor product $[PPh_4]_2$[**4**][9b] (0.067 g, 0.022 mmol).

Conversion of 3a to 3b. CH_2Cl_2 (10 mL) was added to **3a** (0.071 g, 0.06 mmol). The resultant solution was stirred at 30 ^oC for 42 h to give a yellowish-brown solution, which was filtered, followed by removal of the solvent under vacuum. The precipitate was washed with hexanes several times and extracted with CH_2Cl_2, and was then recrystallized with hexanes/CH_2Cl_2 to give a yellowish-brown sample of **3b** (0.052 g, 0.042 mmol) (yield: 70% based on **3a**).

X-ray structural characterization of $[PPh_4]_2$[1], $[PPh_4]_4$[2]·3Et$_2$O, 3a, and 3b·0.5CH$_2$Cl$_2$. Selected crystallographic data for $[PPh_4]_2$[**1**], $[PPh_4]_4$[**2**]·3Et$_2$O, **3a**, and **3b**·0.5CH_2Cl_2 are given in Table 3. All crystals were mounted on glass fibers with epoxy cement. Data collection for $[PPh_4]_2$[**1**] was carried out on a Bruker Nonius Kappa CCD diffractometer and for $[PPh_4]_4$[**2**]·3Et$_2$O, **3a**, and **3b**·0.5CH_2Cl_2 was carried out on a Bruker Apex II CCD diffractometer using graphite-monochromated $Mo_{K\alpha}$ radiation. An empirical absorption correction by the multi-scan method was applied to the data using SADABS.[29] The structures were solved by direct methods and were refined with SHELXL-97/or SHELXL-2014.[30] For $[PPh_4]_2$[**1**], the restraint commands SIMU and DELU were applied to the C56, C57, C69, and C70 atoms for obtaining reasonable thermal parameters. In addition,

the Cu3 and Cu3a atoms were disordered and present in a 67: 33 ratio. For $[PPh_4]_4$[**2**]·$3Et_2O$, the enhanced rigid-bond restraint RIGU was applied to all atoms, along with the ISOR restraint on the C29 atom of the phenyl. Solvent molecules were initially present in structures **2** and **3b**, where all or some of the solvent molecules were disordered. In structure **2**, an Et_2O molecule was chaotically disordered around an inversion centre (0 1/2 1/2). The disordered Et_2O was approximated by arbitrary O21, C72, C73, C74, and C75 positions with partial occupancies (50, 50, 60, 40, and 50%, respectively), totalling one OC_4 for the void. In structure **3b**, one CH_2Cl_2 molecule was disordered between two positions related by an inversion centre and could be modelled easily, in which the C1S, Cl1, and Cl2 atoms were with 50% occupancy, respectively. Except for the disordered O and C atoms on one of the three Et_2O molecules of $[PPh_4]_4$[**2**]·$3Et_2O$, all of the non-hydrogen atoms of $[PPh_4]_2$[**1**], $[PPh_4]_4$[**2**]·$3Et_2O$, **3a**, and **3b**·$0.5CH_2Cl_2$ were refined with anisotropic temperature factors. The selected distances and angles for $[PPh_4]_2$[**1**], $[PPh_4]_4$[**2**]·$3Et_2O$, **3a**, and **3b**·$0.5CH_2Cl_2$ are listed in Table S8. Additional crystallographic data as CIF files are available as Supplementary Information. CCDC reference numbers 1029048 for $[PPh_4]_2$[**1**], 1029049 for $[PPh_4]_4$[**2**]·$3Et_2O$, 1029050 for **3a**, and 1029051 for **3b**·$0.5CH_2Cl_2$.

Acknowledgements

This work was supported by the Ministry of Science and Technology of Taiwan (NSC Grant No. 101-2113-M-003-005-MY3 to M. S.). We are also grateful to the National Center for High-Performance Computing, where the Gaussian and Dmol^3 package and computer time were provided. Professor Hui-Lung Chen at Chinese Culture University is thanked for the discussion of theoretical calculations and Professor Chong Mou Wang at National Taiwan Normal University is thanked for the discussion of electrochemical studies. One of the Reviewers is especially thanked for the assistance in the disordered problem of structures **2** and **3b**. Our gratitude also goes to the Academic Paper Editing Clinic, NTNU.

References

1 (*a*) I. D. Salter, in *Comprehensive Organometallic Chemistry II*, ed. E. W. Abel, F. G. A. Stone and G. Wilkinson, Pergamon, Oxford, 1995, vol. 10, ch. 5, pp. 255─322; (*b*) I. D. Salter, in *Metal Clusters in Chemistry*, ed. P. Braunstein, L. A. Oro and P. R. Raithby, Wiley-VCH: Weinheim, 1999, vol. 1, ch. 1.27, pp. 509─534; (*c*) M. P. Mingos and A. S. May, in *The Chemistry of Metal Cluster Complexes*, ed. D. F. Shriver, H. D. Kaesz and R. D. Adams, Wiley-VCH: New York, 1990, ch. 2, pp. 11─119.

2 (*a*) S. Sculfort and P. Braunstein, *Chem. Soc. Rev.*, 2011, **40**, 2741─2760; (*b*) M. Shieh, C.-Y. Miu, Y.-Y. Chu and C.-N. Lin, *Coord. Chem. Rev.*, 2012, **256**, 637─694.

3 (*a*) J. S. Bradley, R. L. Pruett, E. Hill, G. B. Ansell, M. E. Leonowicz and M. A. Modrick, *Organometallics*, 1982, **1**, 748─752; (*b*) S. M. Draper, A. D. Hattersley, C. E. Housecroft and A. L. Rheingold, *J. Chem. Soc., Chem. Commun.*, 1992, 1365─1367; (*c*) M. A. Beswick, J. Lewis, P. R. Raithby and M. C. Ramirez de Arellano, *J. Chem. Soc., Dalton Trans.*, 1996, 4033─4034; (*d*) M. A. Beswick, J. Lewis, P. R. Raithby and M. C. Ramirez de Arellano *Angew. Chem. Int. Ed. Engl.*, 1997, **36**, 2227─2228; (*e*) M. A. Beswick, J. Lewis, P. R. Raithby and M. C. Ramirez de Arellano, *Angew. Chem. Int. Ed. Engl.*, 1997, **36**, 291─293; (*f*) T. Nakajima, H. Konomoto, H. Ogawa and Y. Wakatsuki, *J. Organomet. Chem.*, 2007, **692**, 5071─5080.

4 (*a*) J. H. Sinfelt, *Bimetallic Catalysts. Discoveries, Concepts, and Applications*, Wiley: New York, 1983; (*b*) P. Braunstein and J. Rosé, *Metal Clusters in Chemistry*, ed. P. Braunstein, L. A. Oro and P. R. Raithby, Wiley-VCH: Weinheim, 1999, vol. 2, ch. 2.2, pp. 616─677; (*c*) J. M. Thomas, B. F. G. Johnson, R. Raja, G. Sankar and P. A. Midgley, *Acc. Chem. Res.*, 2003, **36**, 20─30.

5 (*a*) J. A. Cabeza and P. García-Álvarez, *Organometallics*, 2008, **27**, 2878─2891; (*b*) G. Onodera, H. Matsumoto, Y. Nishibayashi and S. Uemura, *Organometallics*, 2005, **24**,

5799─5801; (*c*) P. Singh and A. K. Singh, *Organometallics*, 2010, **29**, 6433─6442.

6 (*a*) S.-P. Huang and M. G. Kanatzidis, *J. Am. Chem. Soc.*, 1992, **114**, 5477─5478; (*b*) P. C. Liao, J. K. Huang, Y. S. Huang and T. R. Yang, *Solid State Commun.*, 1996, **98**, 279─282; (*c*) Y. Hara, N. Minami and H. Itagaki, *Appl. Catal. A-Gen.*, 2008, **340**, 59─66.

7 (*a*) O. Fuhr, S. Dehnen and D. Fenske *Chem. Soc. Rev.*, 2013, **42**, 1871─1906; (*b*) D. G. MacDonald and J. F. Corrigan, *Philos. Trans. R. Soc. A-Math. Phys. Eng. Sci.*, 2010, **368**, 1455─1472; (*c*) O. Mayasree, C. R. Sankar, K. M. Kleinke and H. Kleinke, *Coord. Chem. Rev.*, 2012, **256**, 1377─1383; (*d*) C. M. Kowalchuk, G. Schmid, W. Meyer-Zaika, Y. Huang and J. F. Corrigan, *Inorg. Chem.*, 2004, **43**, 173─180.

8 (*a*) S. S. D. Brown, S. Hudson, I. D. Salter and M. McPartlin, *J. Chem. Soc.*, *Dalton Trans.*, 1987, 1967─1975; (*b*) B. Kure, S. Ogo, D. Inoki, H. Nakai, K. Isobe and S. Fukuzumi, *J. Am. Chem. Soc.*, 2005, **127**, 14366─14374.

9 (*a*) M. Shieh, M.-H. Hsu, W.-S. Sheu, L.-F. Jang, S.-F. Lin, Y.-Y. Chu, C.-Y. Miu, Y.-W. Lai, H.-L. Liu and J. L. Her, *Chem.─Eur. J.*, 2007, **13**, 6605─6616; (*b*) M. Shieh, Y.-Y. Chu, C.-Y. Miu, P.-F. Wu and T.-M. Zeng, *Dalton Trans.*, 2010, **39**, 1492─1503.

10 D. S. Shephard, T. Maschmeyer, B. F. G. Johnson, J. M. Thomas, G. Sankar, D. Ozkaya, W. Zhou, R. D. Oldroyd and R. G. Bell, *Angew. Chem. Int. Ed. Engl.*, 1997, **36**, 2242─2245.

11 C. E. Anson, L. Ponikiewski and A. Rothenberger, *Z. Anorg. Allg. Chem.*, 2006, **632**, 2402─2404.

12 (*a*) R. D. Adams, B. Captain, W. Fu, P. J. Pellechia and M. D. Smith, *Angew. Chem. Int. Ed. Engl.*, 2002, **41**, 1951─1953; (*b*) R. D. Adams, B. Captain, W. Fu, P. J. Pellechia and M. D. Smith, *Inorg. Chem.*, 2003, **42**, 2094─2101; (*c*) R. D. Adams, B. Captain, P. J. Pellechia and J. L., Jr. Smith, *Inorg. Chem.*, 2004, **43**, 2695─2702.

13 B.-G. Chen, C.-H. Ho, C.-J. Lee and M. Shieh, *Inorg. Chem.*, 2009, **48**, 10757─10768.

14 J. W. Lauher, *J. Am. Chem. Soc.*, 1978, **100**, 5305─5315.

15 L. Ma, S. R. Wilson and J. R. Shapley, *J. Am. Chem. Soc.*, 1994, **116**, 787─788.

16 B. K. Das and M. G. Kanatzidis, *Polyhedron*, 1997, **16**, 3061─3066.

17 G. B. Ansell, M. A. Modrick and J. S. Bradley, *Acta Crystallogr. Sect. C-Cryst. Struct. Commun.*, 1984, **C40**, 365─368.

18 (*a*) M. Xiang, N. Li, R. B. King and H. F. Schaefer, *New J. Chem.*, 2014, **38**, 1433─1440; (*b*) C. Li, J. Xu, J. Zhao, D. Tian and R. B. King, *Dalton Trans.*, 2010, **39**, 10697─10701.

19 (*a*) A. G. Algarra, M. Feliz, M. J. Fernández-Trujillo, R. Llusar, V. S. Safont, C. Vicent and M. G. Basallote, *Chem.─Eur. J.*, 2009, **15**, 4582─4594; (*b*) R. D. Adams, V. Rassolov and Q. Zhang, *Organometallics*, 2013, **32**, 6368─6378.

20 (*a*) V. W.-W. Yam, W.-K. Lee and T.-F. Lai, *Organometallics*, 1993, **12**, 2383─2387; (*b*) V. W.-W. Yam, W.-K. Lee, K.-K. Cheung, B. Crystall and D. Phillips, *J. Chem. Soc., Dalton Trans.*, 1996, 3283─3287; (*c*) V. W.-W. Yam, W. K.-M. Fung and M.-T. Wong, *Organometallics*, 1997, **16**, 1772─1778.

21 (*a*) M. Scheer, A. Schindler, R. Merkle, B. P. Johnson, M. Linseis, R. Winter, C. E. Anson and A. V. Virovets, *J. Am. Chem. Soc.*, 2007, **129**, 13386─13387; (*b*) X. Xue, X.-S. Wang, R.-G. Xiong, X.-Z. You, B. F. Abrahams, C.-M. Che and H.-X. Ju, *Angew. Chem. Int. Ed.*, 2002, **41**, 2944─2946; (*c*) M. S. Doescher, J. M. Tour, A. M. Rawlett and M. L. Myrick, *J. Phys. Chem. B*, 2001, **105**, 105─110.

22 (*a*) A. J. Bard and L. R. Faulkner, *Electrochemical Methods; Fundamentals and Applications,* 2nd ed. John Wiley & Sons: New York, 2001, p. 291; (*b*) T. Nakanishi, H. Murakami, T. Sagara and N. Nakashima, *J. Phys. Chem. B*, 1999, **103**, 304─308.

23 (*a*) C. Creutz, *Prog. Inorg. Chem.*, 1983, **30**, 1─73 and refs. therein; (*b*) D. E.

Richardson and H. Taube, *Coord*. *Chem*. *Rev*., 1984, **60**, 107─129.

24 (*a*) S. Tsukada, Y. Shibata, R. Sakamoto, T. Kambe, T. Ozeki and H. Nishihara, *Inorg*. *Chem*., 2012, **51**, 1228─1230; (*b*) R. Sakamoto, T. Kambe, S. Tsukada, K. Takada, K. Hoshiko, Y. Kitakawa, M. Okumura and H. Nishihara, *Inorg*. *Chem*., 2013, **52**, 7411─7416.

25 P. Kubelka and F. Munk, *Z*. *Tech*. *Phys*., 1931, **12**, 593─601.

26 J. Tauc, *Mater*. *Res*. *Bull*., 1970, **5**, 721─730.

27 D. F. Shriver and M. A. Drezdon, *The Manipulation of Air-Sensitive Compounds*, Wiley-VCH Publishers: New York, 1986.

28 M. G. Simmons, C. L. Merrill, L. J. Wilson, L. A. Bottomley and K. M. Kadish, *J*. *Chem*. *Soc*., *Dalton Trans*., 1980, 1827─1837.

29 Bruker, *SADABS*, Bruker AXS Inc., Madison, Wisconsin, USA, 2003.

30 (*a*) G. M. Sheldrick, *SHELXL97*, version 97-2, University of Göttingen, Germany, 1997; (*b*) G. M. Sheldrick, *Acta Crystallogr*. *Sect*. *A*, 2008, **64**, 112─122.

Table 1 Averaged bond distance (Å) for $[PPh_4]_2$[**1**], $[PPh_4]_4$[**2**]·$3Et_2O$, **3a**, **3b**·$0.5CH_2Cl_2$, and related complexes

complex	Te─Ru	Ru─Ru	Ru─Cu	Cu─Cu	Cu─X[e]	ref
$[PPh_4]_2[TeRu_5(CO)_{14}]$	2.70(2)	2.85(2)				16
$[PPh_4]_2[TeRu_5(CO)_{14}]\cdot CH_2Cl_2$	2.71(4)	2.86(3)				9b
$[PPh_4]_2$[**1**]	2.71(4)	2.88(8) 2.95(6)[b]	2.65(5)	2.54(8)[c] 2.938(4)[d]	2.23(1)	*a*
$[PPh_4]_4$[**2**]·$3Et_2O$	2.71(3)	2.86(5) 2.969(2)[b]	2.66(5)			*a*
3a	2.70(4)	2.90(8) 2.94(6)[b]	2.64(2)			*a*
3b·$0.5CH_2Cl_2$	2.69(2)	2.87(7) 2.94(7)[b]	2.64(3)	2.645(1)[c]		*a*
$[Ph_4As]_2[\{Ru_5C(CO)_{14}\}_2Ag_3Cl]$		2.86(10) 2.95(11)[b]				10
$[Et_4N]_2[\{TeFe_3(CO)_9\}_2Cu_3Br]$				2.71(9)[c] 3.199(2)[d]	2.33(3)	13
$[Et_4N]_2[\{TeFe_3(CO)_9\}_2Cu_3I]$				2.70(2)[c] 3.205(2)[d]	2.50(2)	13
$[PPN]_2[\{Ru_6C(CO)_{16}\}_2Cu_4Cl_2]$		2.90(9) 3.0(2)[b]	2.7(1)	2.675(4)[c] 3.011(4)[d]	2.19(1)	3c
$[Ru_6(CO)_{18}Cu_2(\eta^2\text{-toluene})(\eta^1\text{-toluene})]$		2.90(4) 2.94(3)[b]	2.66(2)			17
$[Ru_6C(CO)_{16}Cu_2(MeCN)_2]$		2.90(8) 3.0(1)[b]	2.65(6)	2.6906(4)[c]		3a

[a] This work. [b] bridged by the Cu or Ag atoms. [c] bridged by the Ru atoms. [d] bridged by the halide atoms [e] X = Cl, Br, and I.

Table 2 Electrochemical data for clusters **1**, **3a**, **3b**, and related complexes

complex	oxidation potential E_{ox}/V[a] ($W_{1/2}$/mV)[b]	comproportionation constant log K_c[c]
1	0.124, 0.184 (217)	1.0
3a	0.134 (119)	
3b	0.154 (120)	
$[TeRu_5(CO)_{14}]^{2-}$[d]	0.090 (96)	
$[TeRu_5(CO)_{14}CuCl]^{2-}$[d]	0.134 (108)	

[a] E_{ox} = from differential pulse voltammetry. [b] ref 22, $W_{1/2}$ = width at half-height, the electronic stoichiometry is determined by the measurement of the peak width at half-height ($W_{1/2}$). [c] ref 23, $RT \ln K_c(X) = nF(\Delta E)$, X corresponded to chemical species and K_c corresponded to the DPV of two successive oxidations, respectively. [d] ref 9b.

Table 3 Crystallographic data for $[PPh_4]_2$[**1**], $[PPh_4]_4$[**2**]·$3Et_2O$, **3a**, and **3b**·$0.5CH_2Cl_2$

	$[PPh_4]_2$[**1**]	$[PPh_4]_4$[**2**]·$3Et_2O$	**3a**	**3b**·$0.5CH_2Cl_2$
empirical formula	$C_{76}H_{40}ClCu_3O_{28}P_2Ru_{10}Te_2$	$C_{146}H_{110}Cu_2O_{41}P_4Ru_{14}Te_4$	$C_{18}H_6Cu_2N_2O_{14}Ru_5Te$	$C_{18.5}H_7ClCu_2N_2O_{14}Ru_5Te$
fw	2954.99	4696.67	1234.28	1276.74
cryst syst	monoclinic	triclinic	monoclinic	monoclinic
space group	$P2_1/n$	$P\bar{1}$	$P2_1/n$	$P121/c1$
crystal dimens, mm	0.21 × 0.17 × 0.04	0.66 × 0.21 × 0.05	0.32 × 0.16 × 0.10	0.38 × 0.30 × 0.08
a, Å	24.3922(6)	14.188(2)	15.2231(3)	14.396(1)
b, Å	14.7256(3)	14.210(2)	10.4337(2)	11.776(1)
c, Å	25.7278 (7)	22.732(3)	19.5749(5)	19.175(2)
α, deg		76.598(9)		
β, deg	110.132(1)	75.207(9)	107.974(1)	105.493(1)
γ, deg		60.659(8)		
V, Å^3	8676.8(4)	3831.6(9)	2957.4(1)	3132.3(5)
Z	4	1	4	4
D (calcd), g/cm^{-3}	2.262	2.035	2.772	2.707
μ, mm^{-1}	3.207	2.471	4.927	4.739
color, habit	black, prism	black, prism	black, prism	black, prism
diffractometer	Nonius (Kappa CCD)	Apex II CCD	Apex II CCD	Apex II CCD
radiation (λ), Å	0.71073	0.71073	0.71073	0.71073
temp, K	298(2)	200(2)	200(2)	200(2)
θ range for data collecn, deg	2.12─25.00	2.71─25.32	2.24─25.05	2.05─25.11
T_{min}/T_{max}	0.61/0.72	0.29/0.89	0.30/0.64	0.27/0.70
no. of indep reflns ($I > 2\sigma(I)$)	8282	6386	4747	4556
no. of parameters	1108	949	381	406
goodness of fit	1.112	0.966	1.068	1.127
R1[a]/wR2[a] ($I > 2\sigma(I)$)	0.091/0.190	0.081/0.164	0.018/0.037	0.028/0.072
R1[a]/wR2[a] (all data)	0.181/0.231	0.185/0.210	0.021/0.039	0.043/0.101

[a] The functions minimized during least-squares cycles were $R1 = \Sigma||F_o| - |F_c||/\Sigma|F_o|$ and $wR2 = [\Sigma[w(F_o^2 - F_c^2)^2]/\Sigma[w(F_o^2)^2]]^{1/2}$.

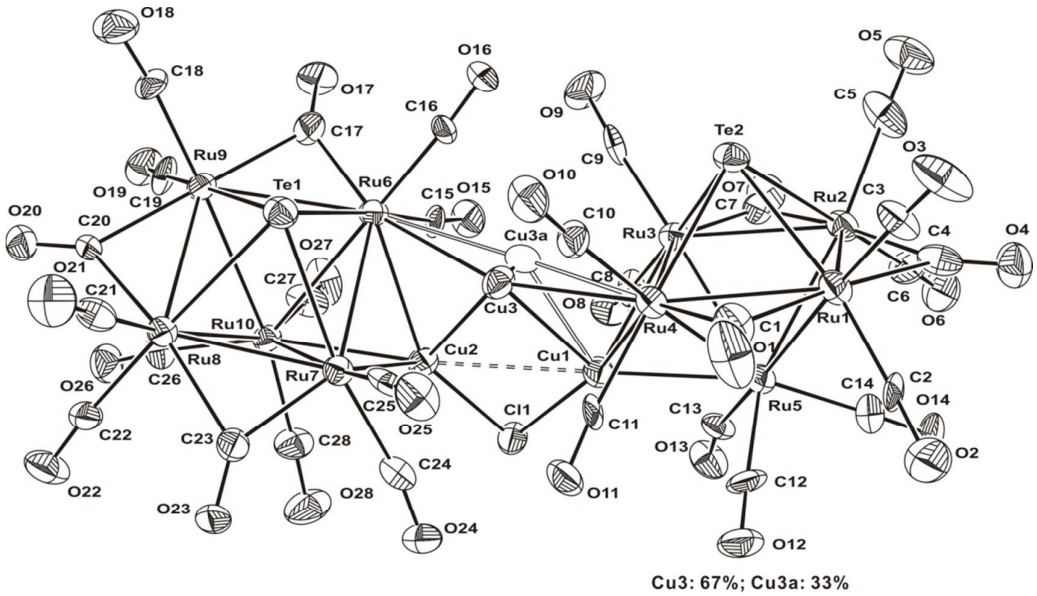

Fig. 1 ORTEP diagram (30% thermal ellipsoids) showing the structure and atom labeling for **1**.

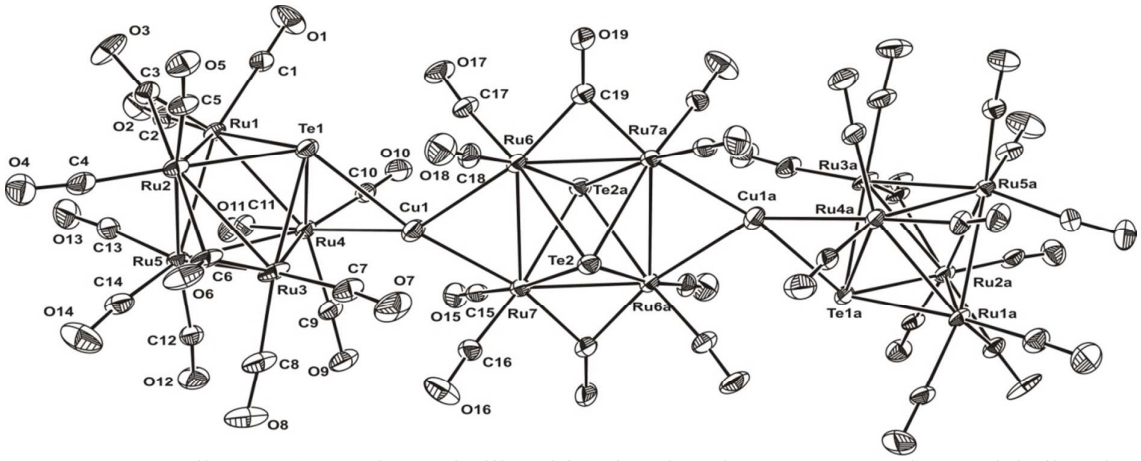

Fig. 2 ORTEP diagram (30% thermal ellipsoids) showing the structure and atom labeling for **2**. The atoms with an additional label (a) are at the equivalent position (2 − x, − y, 1 − z).

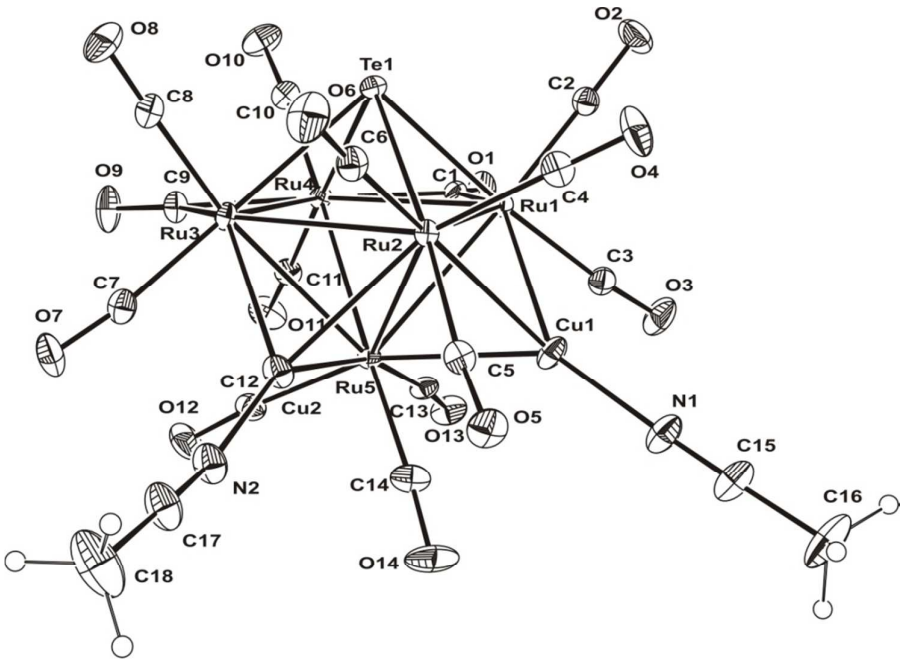

Fig. 3 ORTEP diagram (30% thermal ellipsoids) showing the structure and atom labeling for **3a**.

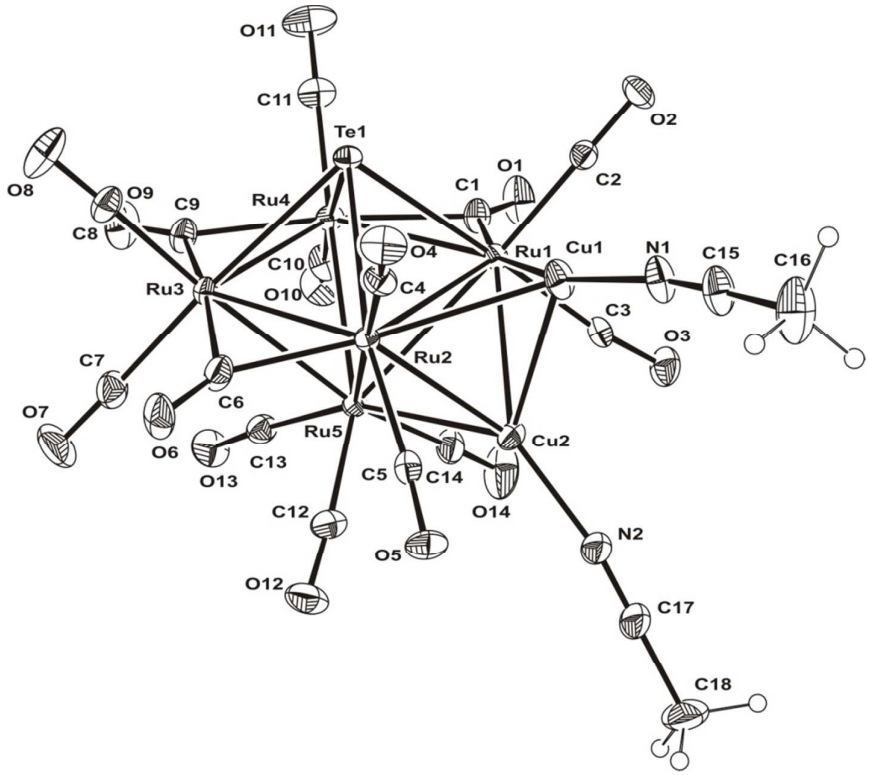

Fig. 4 ORTEP diagram (30% thermal ellipsoids) showing the structure and atom labeling for **3b**.

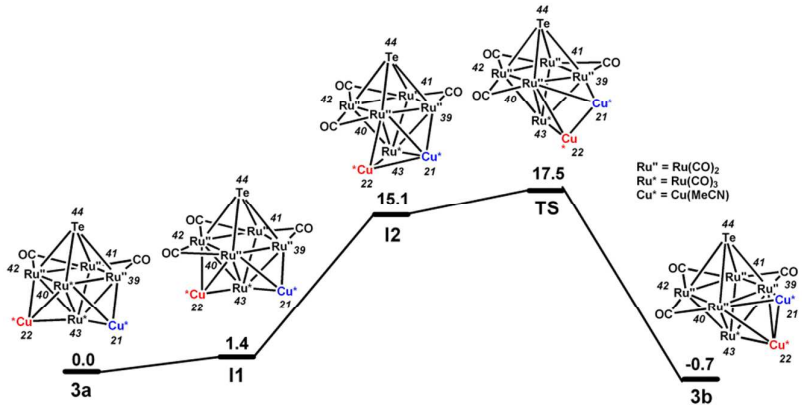

Fig. 5 Free energy profile (kcal mol^{-1}) showing the isomerization of **3a** into **3b**, calculated by MPW1PW91/LanL2DZ.

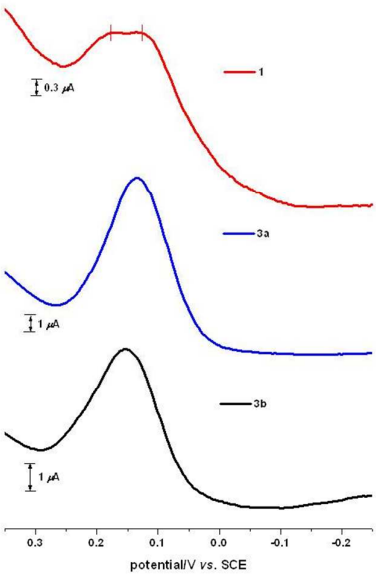

Fig. 6 DPVs in MeCN for **1**, **3a**, and **3b**. Conditions: electrolyte, 0.1 M Bu_4NClO_4; working electrode, glassy carbon; scan rate, 100 mV S^{-1}. Potentials are vs. SCE.

Table of contents entry:

A series of semiconducting Cu_x-incorporated $TeRu_5$-based clusters with differing structural features, facile skeletal arrangements, and effective electronic communication was described.